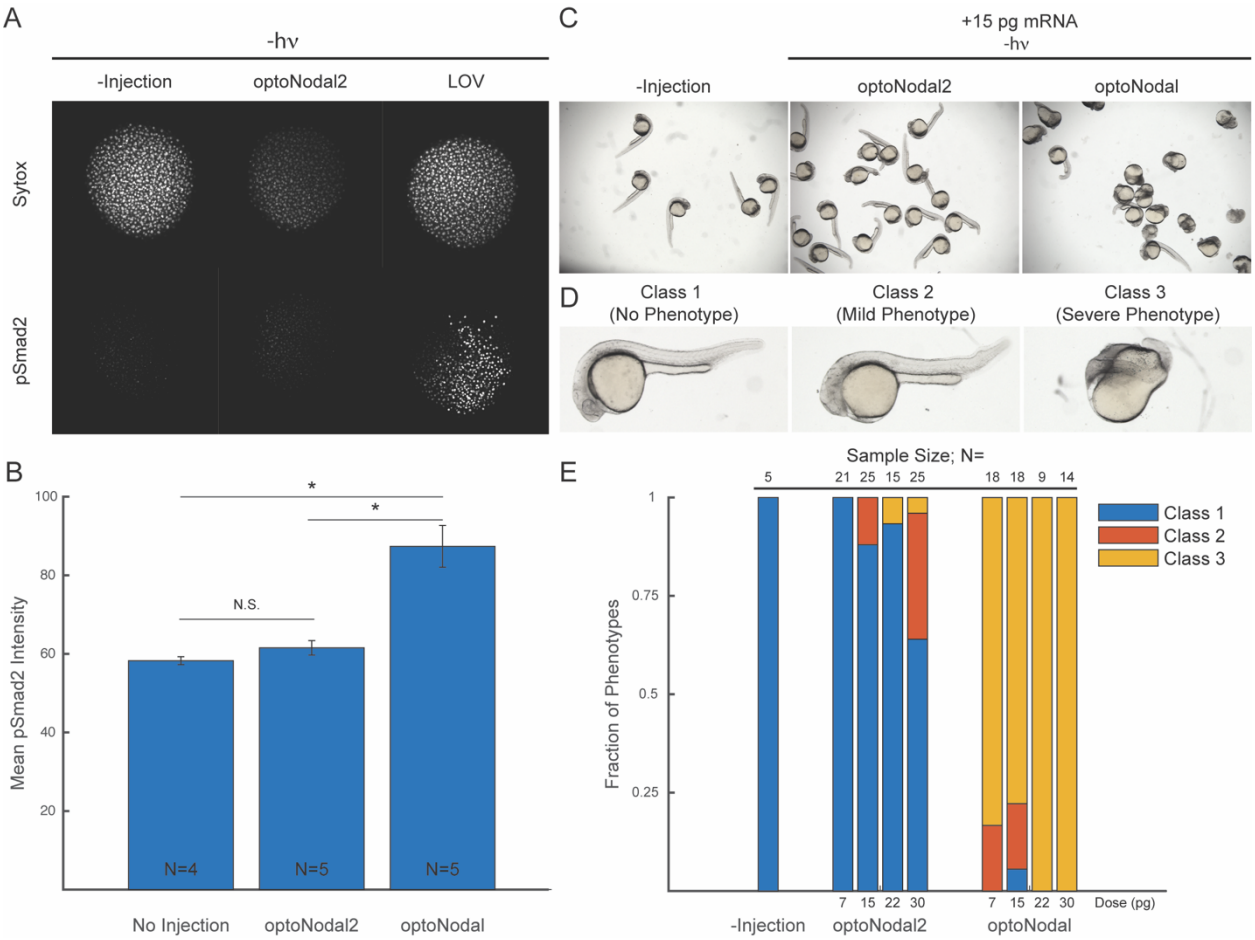

Fig. S1. Comparison of dark activity in optoNodal vs. optoNodal2 reagents. (A) Visualization of dark activity. *Mvg1* embryos were unperturbed ('-Injection') or injected with mRNA encoding Cry-Cib-based optoNodal2 or LOV-based optoNodal receptors. Embryos were raised in the dark until 5.3 hpf, fixed and immunostained for α-pSmad2 (bottom row). (B) Quantification of α-pSmad2 staining intensity in unilluminated embryos. Graph depicts mean α-pSmad2 nuclear staining intensity, and error bars denote s.e.m.. Statistical comparisons between samples were performed with a unpaired sample t-test with asterisks denoting $p < 0.05$. (C) Representative 24 hpf phenotypes of wild-type embryos injected with 15 pg of Cry-Cib or LOV-based optoNodal receptors. (D) Example images denoting phenotypic classes quantified in panel E. Class I embryos exhibit no gross abnormalities, Class II embryos exhibit loss of head structures and/or pronounced axis curvature, Class III embryos exhibit severe dorsalization consistent with excess Nodal signaling activity. (E) Distribution of embryos between phenotypic classes in wild-type embryos without injection or injected with indicated amounts of optoNodal2 or optoNodal receptor mRNAs.

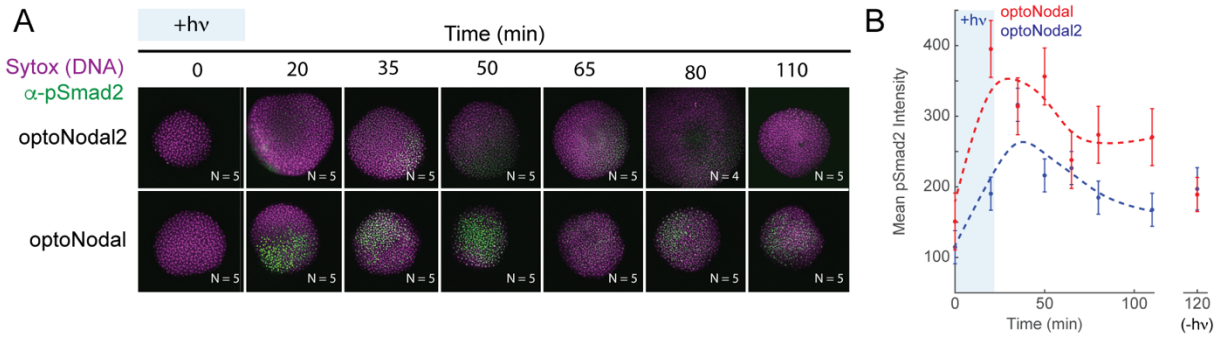

Fig. S2. Dynamic responses of optoNodal and optoNodal2 in MZ*oep* mutants. To confirm the observations of Fig. 1 E,F, the responses of optoNodal and optoNodal2 reagents to a 20 minute impulse of light were measured in MZ*oep* mutant embryos. (A) Measurement of response kinetics for optoNodal (top row) and optoNodal2 (bottom row) reagents. Embryos injected with indicated reagents were illuminated for 20 minutes with 470 nm light. Nodal signaling was measured by α-pSmad2 immunostaining (green). Images are maximum intensity projections of representative embryos. (B) Quantification of Nodal signaling activity from panel A. α-pSmad2 staining intensity was extracted from segmented nuclei in optoNodal (red) and optoNodal2 (blue) treatment groups; each point represents the average nuclear staining intensity from the indicated number replicate embryos in Panel A. Error bars denote the standard error of the mean. Background intensity of unilluminated embryos at the 120 minute timepoint are included (-hν) to indicate baseline levels of signaling activity.

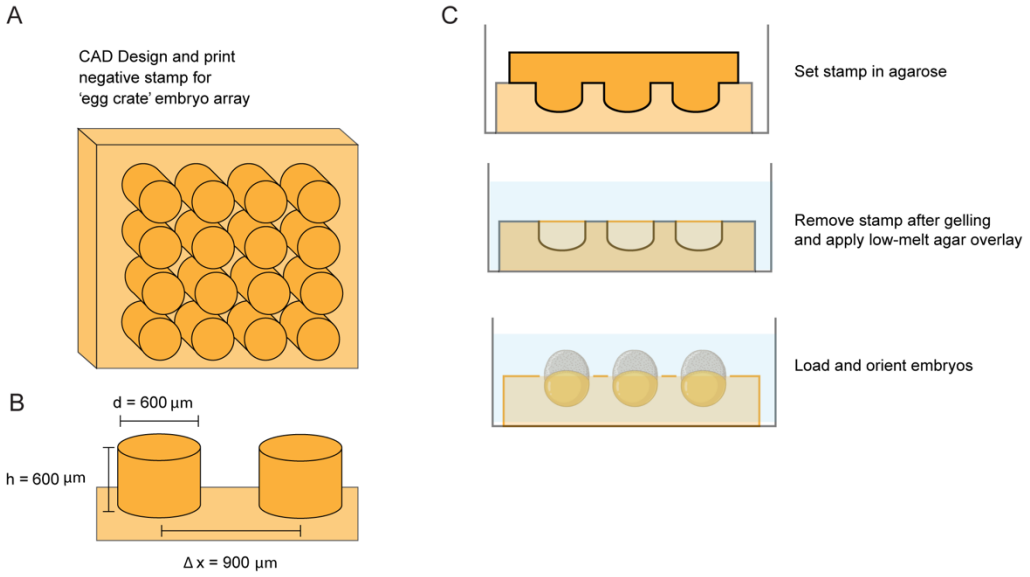

Fig. S3. Design and fabrication of embryo array mounts. (A) Design of embryo array mounts. A negative 'egg crate' stamp consisting of an array of cylindrical posts was designed using TinkerCAD. (B) Typical dimensions of embryo array stamps. For most experiments, an array of cylindrical posts with 600 µm diameter and height (separated by 300 µm in both dimensions) was used. Stamps were 3D printed using a Form 3 SLA printer. (C) Schematic of procedure used to generate agarose embryo mounts from 3D printed stamps. Stamps were pressed into molten 0.5% agarose in embryo medium. After setting, the stamps were manually removed, and an overlay of 0.2% low-melt agarose in embryo medium was pipetted on top at a temperature of ~42 °C. Embryos were then mounted in the devices and manually oriented before the low-melt agarose solidified. Once encased between regular and low-melt agarose, embryos were used for patterning experiments.

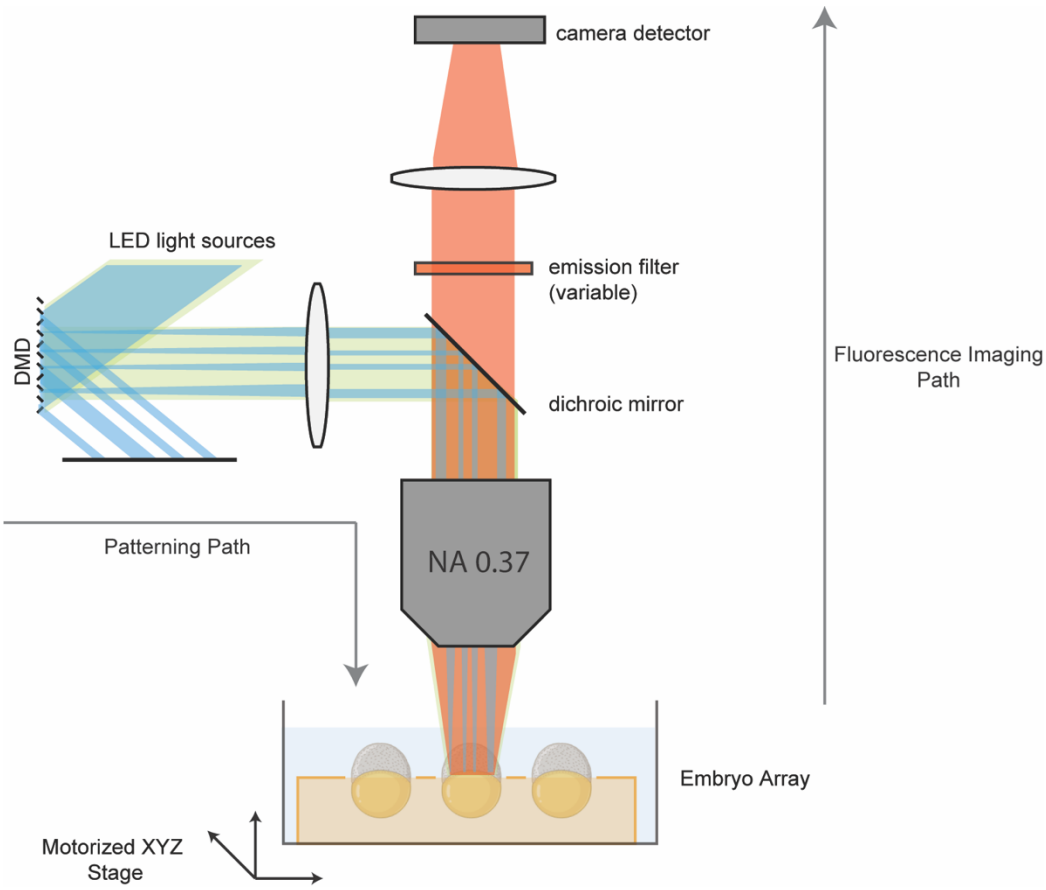

Fig. S4. Design of spatial patterning microscope. Our platform is a modified version of the 'Firefly' microscope design described by Werley *et al*[91] and modified by Farhi *et al*[73]. We modified an Oasis Macro ultra-widefield patterning microscope from Mightex. To create spatial patterns at the sample plane ('Patterning Path'), light from a multi-color LED illuminator is directed to the face of a DMD using a liquid light guide. Pixels on the DMD have two states, 'ON' and 'OFF', with 'ON' pixels directing light toward the sample. Pattern masks are encoded as pixel states on the DMD, and patterned light is collected by a projection lens, reflected off of a multi-band dichroic mirror, and reimaged onto the sample plane using a 4x 0.37 NA objective lens. Emitted light from the sample is collected ('Fluorescence Imaging Path') by the objective lens, passed through the dichroic mirror and a wide-format emission filter on a motorized wheel, and reimaged onto a Hamamatsu Orca Fusion III sCMOS camera by a tube lens. Magnification along the projection path (i.e. from DMD to sample plane) is 2x. Magnification along the imaging path (i.e .from sample plane to camera) is 2x. Sample positioning in three dimensions is controlled via an automated XYZ stage.